Solid-State ^{2}H NMR Studies of Cyclophosphazene Inclusion Compounds: Order and Dynamics of the Benzene Guests

Jorge A. Villanueva-Garibay and Klaus Müller*

Institut für Physikalische Chemie, Universität Stuttgart, Pfaffenwaldring 55, D-70569 Stuttgart, Germany

Received: May 28, 2004; In Final Form: July 15, 2004

Variable-temperature ^{2}H NMR investigations were been carried out to study the molecular behavior of perdeuterated benzene in the inclusion compound with tris(1,2-dioxyphenyl)cyclotriphosphazene. A comprehensive variable-temperature ^{2}H NMR study is presented comprising line shape studies and spin−spin and spin−lattice relaxation experiments. The experimental data clearly indicate the presence of highly mobile guest species at room temperature. Sample cooling gives rise to characteristic line shape effects at around 140 K that can be attributed to a slowing of the rotational motion (nondegenerate three-fold jump processes) of the guest species about the cyclophosphazene channel long axis. The rotation of the benzene molecules about their molecular C_6 axes can be followed to even lower temperatures (∼40 K). A quantitative analysis of the experimental data is achieved by appropriate computer simulations taking into account various motions of the benzene guests. The derived activation energies for the overall rotations are rather small with values of 5.4 ± 0.3 and 4.2 ± 0.1 kJ/mol for motion about the channel long axis and 2.1 ± 0.1 kJ/mol for rotation about the molecular C_6 axis. However, these values are larger than those reported earlier for aliphatic cyclic guests, which directly points to stronger nonbonded guest−host interactions in the present systems. The guest ordering is described by an almost perpendicular orientation of the benzene C_6 axis with respect to the cyclophosphazene channel long axis. The ordering of the benzene guests, which is reduced by fast overall fluctuations of small amplitude, is substantially higher than that observed in related systems, which again can be attributed to the aforementioned guest−host interactions.

Introduction

Inclusion compounds can be formed by various types of organic or inorganic host components.[1,2] Among these, urea and thiourea are well-known representatives. In the presence of suitable guest components, urea and thiourea are able to form hexagonal nanochannels, that are stabilized by hydrogen bonds and that primarily are distinguished by their channel diameters.[3] In fact, the channel size is the main criterion for the selectivity of the enclathrated guests. In the urea channels, elongated molecules such as *n*-alkanes or substituted *n*-alkanes (fatty acids, aldehydes, alcohols, etc.) can be incorporated, whereas thiourea channels have a preference toward bulkier guests, such as cycloalkanes and substituted cycloalkanes.[3,4] Up to now, numerous studies have been reported on urea and thiourea systems that have explored the thermal and structural properties of the host lattice as well as the dynamic features of the guest species.[5−10] The earlier information primarily was deduced from X-ray diffraction, differential scanning calorimetry (DSC), FT IR or NMR spectroscopy,[7−14] whereas solid-state NMR techniques[5,15−19] were employed for the evaluation of the guest dynamics in such inclusion compounds. Among these, ^{2}H NMR methods have demonstrated their particular suitability for the characterization of the molecular guests in such inclusion compounds, yielding information about the molecular conformation, local ordering, and order−disorder phenomena, as well as intra- and intermolecular guest motions.[20−27]

In principle, several dynamic ^{2}H NMR experiments can be employed, each of which is sensitive to a particular time scale for molecular motion. In favorable cases molecular motions over a very broad dynamic range (up to 10 orders of magnitude) can be examined. For instance, line shapes and spin−spin relaxation experiments are used to evaluate motions in the range between 10^4 and 10^8 s^{-1}, whereas spin−lattice relaxation experiments provide information about molecular motions at rate constants of about 10^8−10^{11} s^{-1}. Moreover, slow and ultraslow motions between 10^0 and 10^3 s^{-1} can be studied by stimulated echo and 2D exchange NMR experiments.[28−31]

More recently, inclusion compounds from cyclophosphazene derivatives have registered an increasing interest.[32−37] In contrast to the aforementioned urea and thiourea hosts, cyclophosphazene inclusion compounds are less selective with respect to the enclathrated guest species. Meanwhile, cyclophosphazene inclusion compounds with guest molecules of quite different constitution, such as benzene, benzene derivatives, cycloalkanes, *n*-alkanes, and polymers, are known. It has been shown that the host component also builds up hexagonal channels with an approximate diameter of 4.5−5 Å at its narrowest point in which the guest species are incorporated.[1,2] Unlike the situation for urea and thiourea, in cyclophosphazene inclusion compounds, the host channel structure still remains, even after the guest component has been removed from the host matrix.[23]

^{2}H NMR studies have been reported for cyclophosphazene inclusion compounds with different types of guest compounds.[25,28,38−40] It has been demonstrated that the guest components are highly mobile and undergo various types of intra- and intermolecular motions. However, so far, only a limited number of studies exist in which the guest mobility and

* Corresponding author. Phone: (++49) 711 685 4470. Fax: (++49) 711 685 4467. E-mail: k.mueller@ipc.uni-stuttgart.de.

10.1021/jp047675z CCC: $27.50
Published on Web 08/28/2004

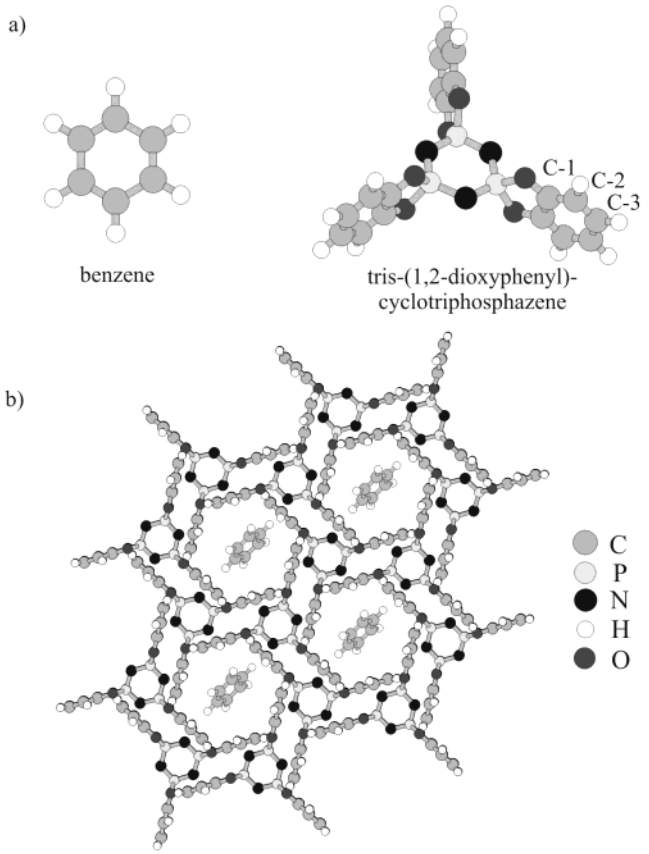

Figure 1. (a) Chemical structures of benzene-d_6 and tris(1,2-dioxyphenyl)cyclotriphosphazene. (b) Schematic drawing of the benzene-d_6/CPZ adduct.

guest ordering have been analyzed and quantified over a large temperature range.[25,28]

In the present work, we report on a solid-state NMR study of the inclusion compound from tris(1,2-dioxyphenyl)cyclotriphosphazene (in the following denoted as cyclophosphazene or CPZ, see Figure 1) with perdeuterated benzene, which addresses the ordering and motional characteristics of the guest species. The sample characterization was done by DSC as well as variable-temperature ^{13}C and ^{31}P NMR spectroscopies. The main part describes a comprehensive ^{2}H NMR investigation in a wide temperature range from 20 K to about room temperature. The variable-temperature experiments comprise ^{2}H NMR line shape studies and spin−spin (T_2) and spin−lattice (T_{1Z}) experiments. From these data, a detailed picture of the molecular features of the guest components (motional contributions, guest ordering) could be obtained. The derived results are discussed in detail and are contrasted with the known data for related systems.

Experimental Section

Materials. Perdeuterated benzene (99 atom % D) and all other chemicals used for the synthetic work were purchased from Sigma-Aldrich Chemicals (Taufkirchen, Germany). Tris(1,2-dioxyphenyl)cyclotriphosphazene was synthesized by the reaction of hexachlorocyclotriphosphazene with catechol in the presence of Na_2CO_3 in THF. The crude product was purified by subsequent washing with diluted HCl and distilled water, followed by vacuum sublimation. Further details can be found elsewhere.[34,41] The inclusion compound of tris(1,2-dioxyphenyl)-cyclotriphosphazene with benzene-d_6 was obtained by direct mixing of the two components in a water bath at 30° C for 0.5 h. Afterward, the inclusion compound was dried for 3 h using a vacuum pump. The quality of the inclusion compound was checked by DSC and ^{13}C and ^{31}P MAS NMR spectroscopy. The guest/host ratio was found to be approximately 8:1.

NMR Measurements. All ^{2}H NMR measurements were carried out on a Bruker CXP 300 spectrometer (Bruker/Rheinstetten) operating at a frequency of 46.07 MHz for deuterium (magnetic field strength = 7.04 T), equipped with a Tecmag control unit. The ^{2}H NMR measurements above 110 K were done by using a standard (liquid nitrogen flow) Bruker 5-mm double-resonance probe and a $\pi/2$ pulse length of 2 μs. For the low-temperature ^{2}H NMR experiments ($T \leq 110$ K), a Bruker 5-mm single tuned probe ($\pi/2$ pulse width = 4.5 μs) coupled to a liquid helium flow cryostat (Oxford Instruments) was used. The variable-temperature ^{2}H NMR spectra were recorded by applying the quadrupole echo sequence $[(\pi/2)_x-\tau_e-(\pi/2)_y-\tau_e-\text{acquisition}]$ with a constant time interval of $\tau_e = 20$ μs. The spin−spin relaxation times (T_2) and the corresponding partially relaxed spectra were obtained by using the same sequence but changing the interval τ_e between the $\pi/2$ pulses. All spin−spin relaxation times T_2 are powder values that were derived from the τ_e dependence of the quadrupole echo maximum. In general, nonexponential echo decays occur. The given T_2 values define the time at which the echo decayed to 1/e of its value at $\tau_e = 20$ μs. A modified inversion recovery sequence $[\pi-\tau_r-(\pi/2)_x-\Delta-(\pi/2)_y-\Delta-\text{acquisition}]$ was employed for the determination of the spin−lattice relaxation times (T_{1Z}). Here, the pulse spacing $\Delta = \tau_e$ was set to 20 μs, whereas τ_r varied in the range of milliseconds to several seconds. All recycle delays were selected to be at least 10 times the spin−lattice relaxation time T_{1Z} and ranged from 0.5 ms to 10 s depending on the actual temperature. Again, the spin−lattice relaxation times T_{1Z} are powder values that were derived from the τ_r dependence of the detected NMR signal after inversion. During the inversion recovery experiments, only exponential decays were registered. Appropriate phase cycling was employed to eliminate quadrature phase errors. The number of scans varied between 256 and 1024 depending on the S/N ratio. The sample temperature above 110 K was controlled by a Bruker BVT 1000 unit, whereas at $T \leq 110$ K, a ITC 4 temperature control unit from Oxford Instruments was used. In general, for both controllers the accuracy of the temperature was found to be within ±1 K.

^{13}C and ^{31}P MAS NMR spectra were recorded at 75.47 and 121.5 MHz, respectively, on an MSL 300 Bruker spectrometer (magnetic field strength = 7.05 T) using a standard 4-mm Bruker MAS probe. All MAS experiments were done at a sample spinning rate of 5 kHz applying either single-pulse or cross-polarization (CP) excitation (contact time = 3 ms). The $\pi/2$ pulse widths for carbon, phosphorus, and protons were 4 μs. Recycle delays were chosen to 6 s for ^{13}C and between 15 and 60 s for ^{31}P NMR experiments. ^{13}C and ^{31}P chemical shifts were determined relative to the external standards adamantane (^{13}C) and H_3PO_4 (^{31}P). The ^{13}C chemical shifts were then expressed relative to TMS ($\delta = 0$ ppm).

Differential Scanning Calorimetry. Calorimetric studies were performed with a differential scanning calorimeter, model Netzsch DSC 204 (Netzsch/Selb), under nitrogen flow at heating rates of 10 °C/min.

Data Processing. Processing of the experimental and simulated NMR signals was performed on a SUN Sparc 10 workstation using the NMRi and Sybyl software packages (Tripos, St. Louis). The given T_2 and T_{1Z} data represent powder

average values that were derived from the amplitudes of the free induction decays from the respective experiments.

Simulations. The theoretical simulations presented here were done with appropriate FORTRAN programs, developed in our group for the behavior of an isolated $I = 1$ spin system in different types of dynamic NMR experiments.[14,28] The simulation programs are very general and take into account various types of molecular motions of the system under investigation. A numerical diagonalization of the corresponding relaxation matrices using standard packages gives the theoretical line shapes and relaxation times.[42] In all simulations, the final best fit was chosen by direct comparison between experimental and theoretical spectra, taking into account the overall line shapes as well as the relative amplitudes.

The basic theory of dynamic ^{2}H NMR spectroscopy is well documented. In the following, we briefly review only those points that are of relevance for the present data analysis. As outlined elsewhere, the free induction decay starting at the top of the quadrupole echo is given by[5,15,17−19,43,44]

$$S(t,2\tau_e) = \mathbf{1}\exp(\mathbf{A}t)\exp(\mathbf{A}\tau_e)\exp(\mathbf{A}\tau_e)^*\,\mathbf{P}(0) \qquad (1)$$

Here, the vector $\mathbf{P}(0)$ contains the fractional populations of the N exchanging sites in thermal equilibrium. $\mathbf{A}$ denotes a square complex matrix of size N with

$$\mathrm{A} = \mathrm{i}\Omega + \mathrm{K} \qquad (2)$$

The imaginary part of $\mathbf{A}$ is given by the diagonal matrix Ω whose elements ω_{ii} describe the frequencies of exchanging sites. The real part corresponds to the kinetic matrix $\mathbf{K}$. The nondiagonal elements k_{ij} are the jump rates from site j to i, while the diagonal elements k_{ii} represent the sum of jump rates for leaving site i and the residual line width $1/T_2^0$. Depending on the complexity of the system under examination, several independent intermolecular or internal processes can be superimposed in this way. In the present study, the size of the largest matrix is 18, accounting for three sites for the three-fold jumps about the channel main axis and six sites for rotation about the molecular C_6 axis.

The correlation times τ_c for a jump process follow the detailed balance and are related to the rate constants k_{ij} by

$$\frac{1}{\tau_c} = \frac{k_{ij}}{p_i} \qquad (3)$$

where p_i is the equilibrium population of site i.

The simulation of the partially relaxed ^{2}H NMR spectra from the modified inversion recovery experiment was feasible using eqs 4−6. Here, the detected signal $S(t,2\tau_e,\tau_r)$ can be represented by

$$S(t,2\tau_e,\tau_r) = [1 - 2\exp(-\tau_r/T_{1Z})]S(t,2\tau_e) \qquad (4)$$

where $S(t,2\tau_e)$ is the FID signal from the earlier quadrupole echo experiment (see eq 1). The delay τ_r corresponds to the relaxation interval between the inversion pulse and the quadrupole echo sequence.

The spin−lattice relaxation times T_{1Z}, which in the most general case exhibit a distinct orientational dependence, were calculated on the basis of a dominant quadrupolar interaction. In this case, T_{1Z} is related to the spectral densities by[45−47]

$$\frac{1}{T_{1Z}} = \frac{3}{16}\left(\frac{e^2qQ}{\hbar}\right)^2 [J_1(\omega) + 4J_2(2\omega)] \qquad (5)$$

The spectral densities, J_m, were derived by solving eq 5 for a general N-site exchange[48,49]

$$J_m(\omega) = 2\sum_{a,a'=-2}^{2} d^{(2)}_{ma}(\theta')d^{(2)}_{ma'}(\theta')\sum_{n,l,j=1}^{N} X_l^{(0)}X_l^{(n)}X_j^{(0)}X_j^{(n)}\, d^{(2)}_{0a}(\theta''_l)d_{0a}{}^{(2)}(\theta''_j)\cos(a\phi_l - a\phi_j)\frac{\lambda_n}{\lambda_n{}^2 + \omega^2} \qquad (6)$$

with

$$\phi_i = \phi_i'' - \phi'$$

Here, $\mathbf{X}^{(n)}$ and λ_n are the corresponding eigenvectors and eigenvalues of the symmetrized rate matrix $\mathbf{K}'$; θ'' and ϕ'' are the spherical polar angles between the principal axis and an intermediate axis (motional axis) system; and the angles θ' and ϕ' connect the intermediate and laboratory axis systems. $d^{(2)}_{ab}(\theta)$ represents elements of the reduced Wigner rotation matrix.

On the basis of eqs 4−6, it is possible to simulate partially relaxed spectra (inversion recovery experiment) in the presence of both spin−lattice and spin−spin relaxation contributions. Here, the angle-dependent T_{1Z} values (spin−lattice relaxation effects) are calculated via eqs 5 and 6, while the spin−spin relaxation effects (i.e., line broadening effects) are accessible by solving eq 1.[50] The two contributions are then combined by eq 4.

Motional Models. In the present work two major motional contributions of the benzene guests have to be discussed that affect the ^{2}H NMR data, namely rotation about the guest symmetry axis, and reorientational motion within the host channels. For the latter contribution several potential mechanisms were taken into consideration, such as a combination of rotational jumps motions with overall fluctuations, jump motions within an ordering potential, restricted overall rotations, etc. Eventually, it turned out that the line shape effects and spin relaxation at best can be reproduced by a rotation about the molecular C_6 axis (degenerate six-site jump process), and a rotation about the channel long axis (nondegenerate three-site jump process) with the populations p_1, p_2, and p_3 ($p_1 + p_2 + p_3 = 1$, $p_1 \geq p_2 = p_3$).

In addition, as outlined below, a Gaussian distribution for the correlation times was used to achieve a better reproduction of the partially relaxed ^{2}H NMR line shapes (quadrupole echo experiment) in the intermediate temperature range between 110 and 180 K. The Gaussian distribution is given by

$$g(\tau_c - \tau_{c,0}) = \frac{1}{\sqrt{2\pi}\sigma}\exp\left\{-\frac{[\log(\tau_c/\tau_{c,0})]^2}{2\sigma^2}\right\} \qquad (7)$$

where σ and $\tau_{c,0}$ are the width and center of the distribution, respectively. The upper and lower limits of the correlation times were taken to 10^{-10} and 10^{-2} s, respectively. To obtain a uniform and smooth Gaussian distribution, the whole correlation time scale was subdivided into equidistant parts (i.e., 12 parts for each order of magnitude). The ^{2}H NMR signals were then calculated by the summation of the whole series of spectra for a given center of the distribution $\tau_{c,0}$ and a given distribution width σ.

Results and Discussion

In the present study, variable-temperature ^{2}H NMR experiments were performed on the benzene-d_6/tris(1,2-dioxyphenyl)-cyclotriphosphazene inclusion compound (benzene-d_6/CPZ) in

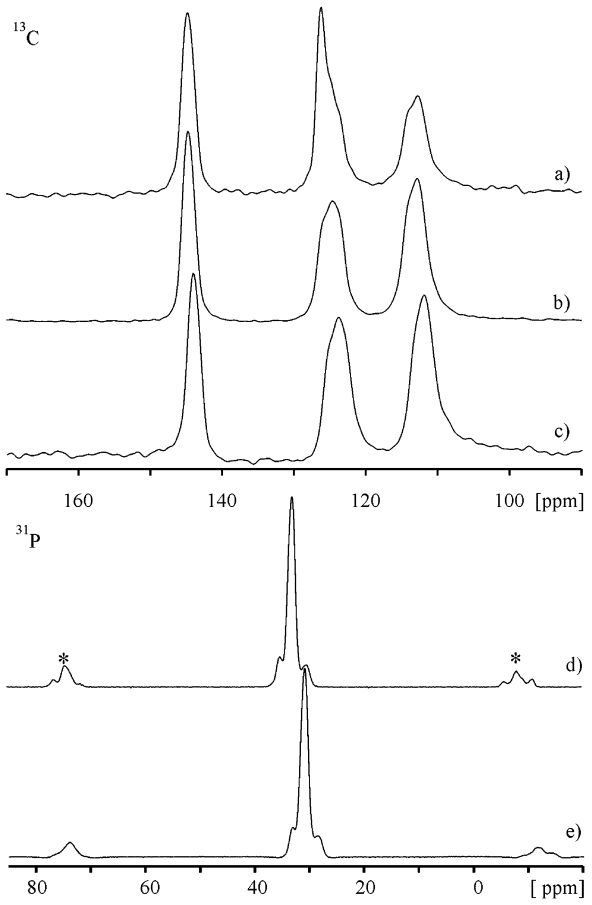

Figure 2. ^{13}C MAS NMR spectra of benzene/cyclophosphazene: (a) single pulse sequence at $T = 300$ K, (b) CP sequence at $T = 300$ K, and (c) CP sequence at $T = 147$ K. ^{31}P CP MAS NMR spectra at (d) $T = 300$ K and (e) $T = 147$ K. (Asterisks mark the spinning sidebands.)

the temperature range between 20 and 300 K. Prior to the ^{2}H NMR studies, the sample was examined by DSC and ^{13}C and ^{31}P CP MAS NMR spectroscopies. The DSC traces for cyclophosphazene inclusion compounds exhibit two exothermic peaks that can be attributed to a first-order solid−solid phase transition at 503 K and a melting peak at 518 K. The first phase transition was described by Allcock[51] and is due to the coexistence of monoclinic and hexagonal crystal cells at higher temperatures. DSC measurements between 120 K and room temperature did not give any evidence for additional low-temperature solid−solid phase transitions of the benzene-d_6/CPZ inclusion compound.

In Figure 2, three representative ^{13}C MAS NMR spectra of benzene-d_6/CPZ are displayed. In general, relatively broad ^{13}C NMR lines are visible, as discussed previously by Comotti et al.[52] They suggest that empty cyclophosphazene channels must be present as well, which are a result of the pumping during sample preparation.[35,36,53] The ^{13}C NMR spectra in Figure 2 exhibit four signals that refer to carbons C-1 (145 ppm), C-2 (124 ppm), and C-3 (112 ppm) of the phenyl ring of the CPZ host and to the benzene carbons (peak at 126 ppm). The latter signal clearly can be separated by the comparison of the ^{13}C NMR spectra from single-pulse excitation and CP experiments (see spectra a and b). The change of the relative signal intensities for the guest and host components is related to the high guest mobility and to the absence of protons in the perdeuterated guest molecules. Therefore, cross-polarization is less efficient for the carbon nuclei of the benzene guests. The spectra recorded at

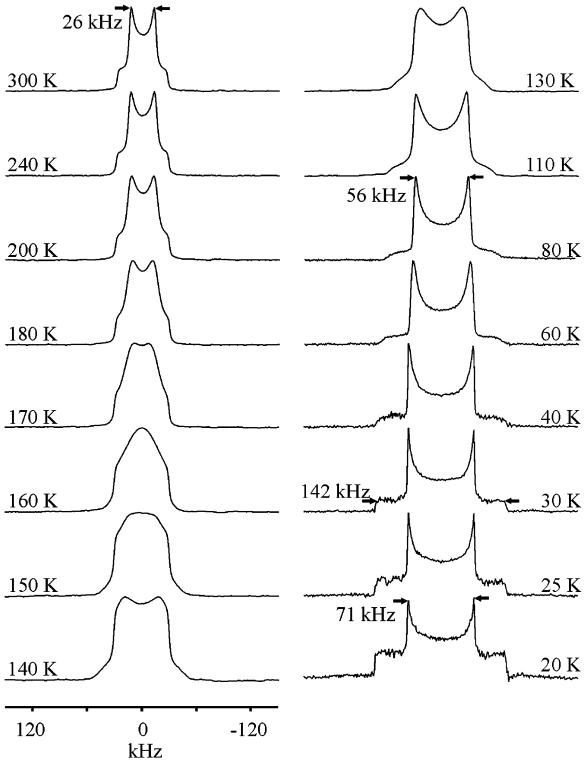

Figure 3. Variable-temperature ^{2}H NMR line shapes for the benzene-d_6/CPZ inclusion compound with a pulse spacing of $\tau_e = 20$ μs.

300 and 147 K—apart from a small temperature dependence of the ^{13}C chemical shift—are practically identical (see spectra b and c), which implies the absence of any significant structural alteration of the CPZ host channels within the temperature range covered here.

Figure 2 also contains ^{31}P CP MAS NMR spectra of the same sample that were recorded at 147 and 300 K (spectra d and e). The ^{31}P NMR spectra exhibit a characteristic asymmetric splitting centered at 33 ppm due to the dipolar coupling between the ^{31}P and ^{14}N nuclei that is not completely suppressed by magic-angle sample spinning.[54] As for the ^{13}C NMR spectra, the ^{31}P NMR spectra give no evidence for structural changes of the CPZ host lattice between 147 K and room temperature. The experimental ^{31}P NMR spectra are consistent with the hexagonal symmetry of the CPZ channels, where all phosphorus atoms are equivalent in the unit cell. Comotti et al.[52] reported that the ^{31}P CP MAS NMR spectrum for monoclinic CPZ consists of three signals at 38.3, 35.1, and 32.0 ppm, which definitively are not observed for the present sample.

The following part describes variable-temperature ^{2}H NMR studies on benzene-d_6/CPZ, which provide valuable information about the mobility and ordering behavior of the benzene guest. On the basis of the observed line shape effects, we made a separation into (i) high ($T > 180$ K), (ii) intermediate (110 K $\leq T \leq 180$ K), and (iii) low ($T < 110$ K) temperature ranges. It should be emphasized that this separation is arbitrary and—as already shown by the aforementioned DSC, ^{13}C and ^{31}P NMR studies—is not connected to a detectable phase transition.

Figure 3 depicts a representative series of variable-temperature ^{2}H NMR spectra for benzene-d_6/CPZ. In the high temperature range, axially symmetric ^{2}H NMR line shapes are detected. Here, the benzene guests are highly mobile, as can be determined from the quadrupolar splitting between the perpendicular singularities of $\Delta\nu_\perp = 26$ kHz observed at 300 K. This value is considerably smaller than the value of 142 kHz for

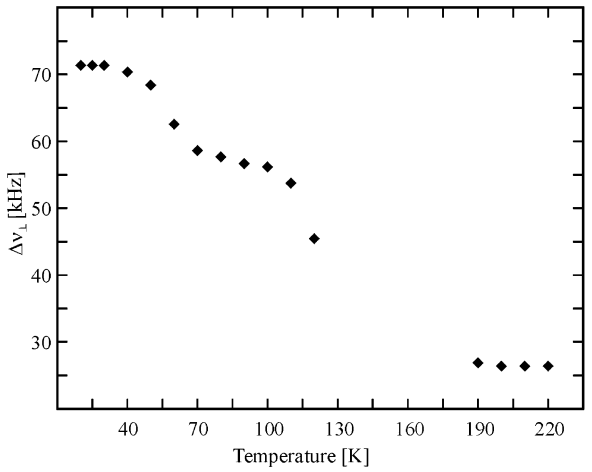

Figure 4. Experimental quadrupolar spitting ($\Delta\nu_\perp$) as a function of temperature for benzene-d_6/CPZ.

completely rigid guest molecules, assuming a static quadrupolar coupling constant $\nu_{Q,stat}$ of 189 kHz (aromatic C$-^2$H bonds). The temperature dependence of the experimental quadrupolar splitting is shown in Figure 4, which reveals three characteristic plateau regions within the temperature range covered here. Upon lowering of the sample temperature, the quadrupolar splitting remains constant until 200 K. In the intermediate temperature region, the overall ^{2}H NMR pattern is found to vary continuously with temperature. Here, typical line shape effects occur, until an axially symmetric ^{2}H NMR spectrum (quadrupolar splitting $\Delta\nu_\perp = 56$ kHz) again is observed at 110 K. At temperatures below 110 K, $\Delta\nu_\perp$ increases continuously until it again reaches a plateau value of 71 kHz at 30 K. This value is still a factor of 2 smaller than the aforementioned "rigid limit" value. In addition, at temperatures below 40 K, an additional broader spectral component grows in with a splitting of 142 kHz that stems from completely immobile benzene guests in the CPZ channels.

On the basis of the molecular symmetries of the guest molecules and host channel and with the findings from earlier studies on the same and related compounds,[25,28,38] it is possible to discuss the observed ^{2}H NMR line shape effects in a qualitative way. At very low temperatures ($T \geq 20$ K), the benzene molecules become mobile and rotate about their molecular C_6 axes. This guest motion reduces the quadrupolar splitting by a factor of $^1/_2$, because the angle Θ_1 between the C$-^2$H bond direction and the motional symmetry axis is 90°. With the well-known equation for the motionally averaged quadrupolar splitting (for a highly symmetric rotational motion)[15]

$$\langle\Delta\nu\rangle = \frac{3}{4}\nu_{Q,stat}\frac{1}{2}(3\cos^2\Theta_1 - 1) \qquad (8)$$

and with a static quadrupolar coupling constant of $\nu_{Q,stat} = 189$ kHz, we obtain a value of $\langle\Delta\nu\rangle = 71$ kHz, as found experimentally. The fact that rigid and mobile benzene guests coexist up to about 30 K might indicate some sample heterogeneity or a distribution of motional correlation times for the rotation about the C_6 symmetry axis, as also discussed elsewhere.[55] The additional reduction of the spectral splitting up to 80 K can be understood by the onset of a fast wobbling motion. The characteristic line shape effects above 110 K are attributed to an additional efficient overall reorientational motion of the guest molecules about the CPZ channel long axis, as also discussed in an earlier study on the same compound and related systems.[25,28,38]

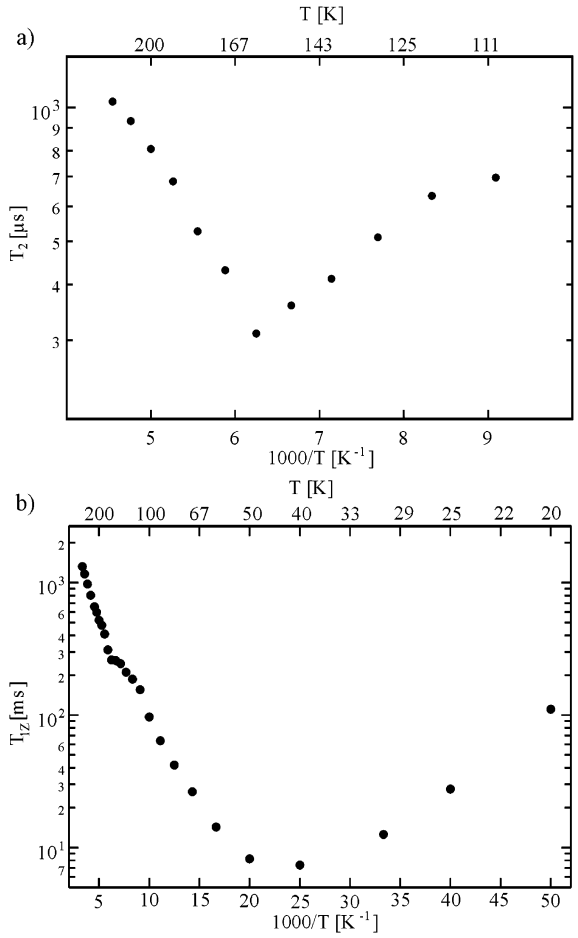

Figure 5. Experimental ^{2}H NMR (a) spin−spin relaxation times and (b) spin−lattice relaxation times for benzene-d_6/CPZ.

For a quantitative analysis of the underlying guest motions, additional spin−spin and spin−lattice relaxation experiments were performed. Figure 5 summarizes the experimental spin−spin and spin−lattice relaxation curves of the present sample. The spin−spin relaxation experiments were performed to support the line shape analysis in the intermediate temperature range between 110 and 180 K. The experimental T_2 curve exhibits a characteristic minimum at about 160 K, which marks the temperature at which the motional rate constant is on the order of the modulated quadrupolar interaction. Such T_2 minima, arising from irreversible loss of phase coherence in the presence of molecular motions, are well-known. They have been reported earlier, for instance, during studies of electron spin[56,57] and quadrupolar echoes.[18,44,58]

In addition, in Figure 6, three representative series of partially relaxed spectra (quadrupole echo experiment) are provided. It can be seen that the line shapes exhibit characteristic changes with the actual pulse spacing τ_e, which reflect the specific T_2 anisotropy due to the underlying molecular motion. Likewise, for the experimental T_{1Z} curve a minimum is found at 40 K along with some characteristic inflections at higher temperatures, which will be further discussed below.

To reproduce the present ^{2}H NMR line shape effects and spin−spin relaxation data, various types of motional models for the dynamics of perdeuterated benzene guests were examined. As mentioned earlier, the experimental ^{2}H NMR data at best could be described by the assumption of two superimposed, dominant motional contributions, namely, spinning about the

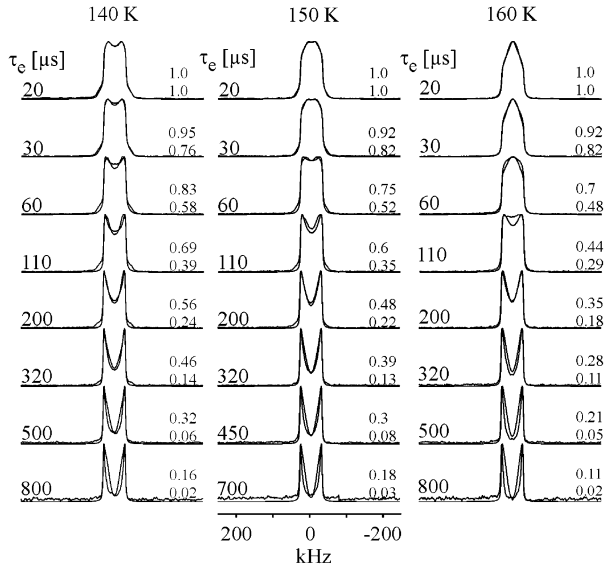

Figure 6. Partially relaxed ^{2}H NMR spectra obtained from the quadrupole echo sequence at the most relevant temperatures around the T_2 minimum. The plot shows a superposition of the experimental and simulated spectra for different τ_e values. All spectra are plotted to the same amplitude. The numbers given to the right of every data set are the scaling factors (upper number, experiment; lower number, simulation). The Euler angle Θ_2 was taken to 85° (140, 150, and 160 K).

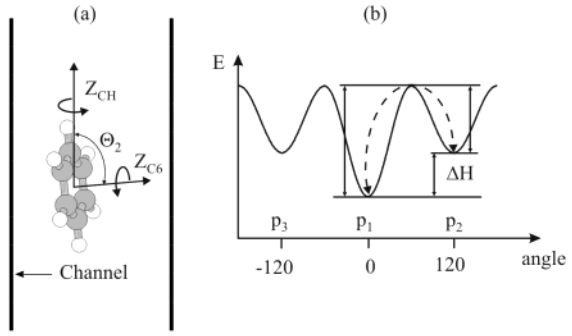

Figure 7. (a) Schematic drawing of the proposed benzene motions. The motional symmetry axis Z_{CH} is assumed to point along the channel long axis. (b) Potential energy profile for the three-site jump model. The equilibrium populations of the sites follow the order $p_1 \geq p_2 = p_3$; $p_2 = {}^1/_2(1 - p_1)$.

benzene hexad axis[59] (Z_{C6}) and rotation about the CPZ channel symmetry axis[21,60] (Z_{CH}), as depicted in Figure 7.

The influence of the two molecular contributions on the ^{2}H NMR line shapes is demonstrated in Figure 8 by a series of theoretical spectra. These simulations account for a C_6 rotation by a degenerate six-fold jump process, whereas for the rotation about the channel axis, a degenerate three-fold jump process was assumed.[38] The two motional symmetry axes are oriented perpendicular with respect to each other (angle $\Theta_2 = 90°$). Here, within the rows, the correlation time for the rotation about the channel axis is varied, whereas within each column, the correlation time for the C_6 rotation changes. It can be seen that the experimental line shape effects between 110 and 180 K of the benzene-d_6/CPZ inclusion compound resemble the theoretical spectra in Figure 8 in the limit of a fast rotation about the molecular C_6 axis and a thermally activated rotation about the CPZ channel axis (as depicted by the spectra of the upper row). However, it should be noted that a final proof for the absolute orientation of the motional symmetry axis Z_{CH} with respect to the channel long axis cannot be given, because we only work

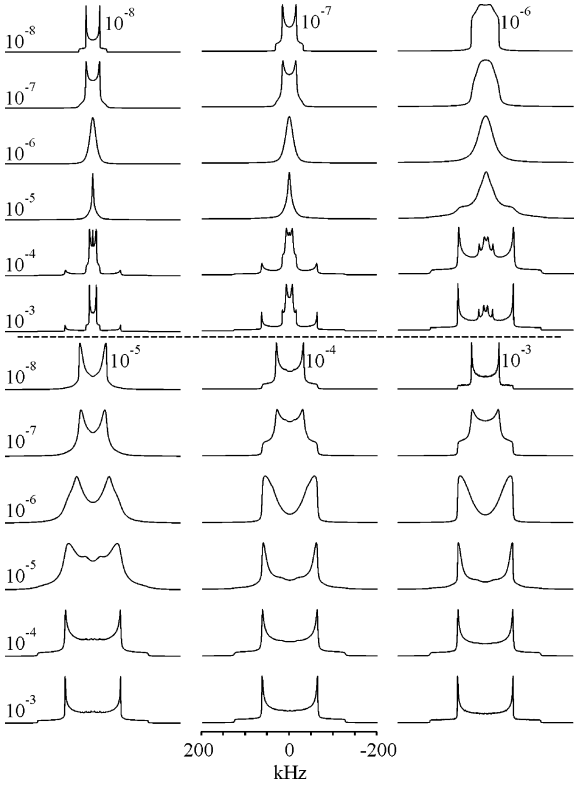

Figure 8. Theoretical ^{2}H NMR line shapes (quadrupole echo, $\tau_e = 20$ μs) for two superimposed jump processes with the correlation times given in the figure (rows, correlation times for the rotation about the first motional axis, degenerate six-site jumps; columns, correlation times for the rotation about the second motional axis, degenerate three-site jumps). The two motional symmetry axes are oriented perpendicular with respect to each other ($\Theta_2 = 90°$).

on a powder sample. Nevertheless, on the basis of the spatial restrictions imposed by the CPZ lattice, the proposed motional model appears to be very likely.

During the data analysis, it turned out that the degenerate three-fold jump model for the benzene motion about the CPZ channel axis cannot fully account for all experimental line shapes in the intermediate temperature range, as shown in Figure 3. In particular, the model is not appropriate in the slow motional range (spectra at 140 and 150 K), where some shoulders are registered in the experiment, that are always missing in the computer simulations. For this reason, a nondegenerate three-site jump model, i.e., jumps between unequally populated sites, was introduced. In Figure 9, theoretical ^{2}H NMR spectra are depicted that are obtained with a three-fold jump model, a correlation time $\tau_{CH} = 8 \times 10^{-7}$ s ($\tau_{C6} < 10^{-8}$ s), and the relative populations p_1 ($p_1 \geq p_2 = p_3$), as indicated. The given examples clearly demonstrate that the actual population p_1 has a significant influence on such dynamic ^{2}H NMR line shapes. These theoretical spectra should also emphasize the influence of the pulse separation time τ_e of the quadrupole echo experiment. That is, for a quantitative data analysis, the consideration of the finite pulse separation τ_e is absolutely mandatory.

The opening angle Θ_2 between the two motional symmetry axes represents another adjustable parameter for the present line shape analysis. In Figure 10 (left column), representative ^{2}H NMR line shapes are depicted that refer to different opening angles again and correlation times $\tau_{CH} = 2 \times 10^{-6}$ s, $\tau_{C6} < 10^{-8}$. It can be seen that the actual opening angle Θ_2 has a considerable impact on the overall appearance of the theoretical ^{2}H NMR spectra. Extensive model simulations have shown that,

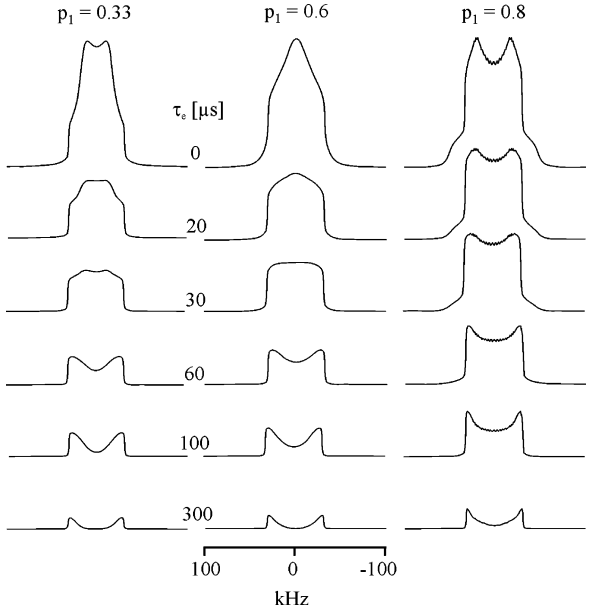

Figure 9. Influence of the equilibrium population p_1 on the theoretical partially relaxed ^{2}H NMR line shapes (quadrupole echo sequence). The simulations are based on two superimposed rotational processes. The first rotation is a degenerate six-site jump process in the fast motional limit (angle from the C$-^2$H bond direction $\Theta_1 = 90°$). The second rotation is a nondegenerate three-site jump in the intermediate range with $\tau_c = 8 \times 10^{-7}$ s and the populations given in the figure (angle between the two motional axes $\Theta_2 = 90°$). The quadrupolar coupling constant is 169 kHz.

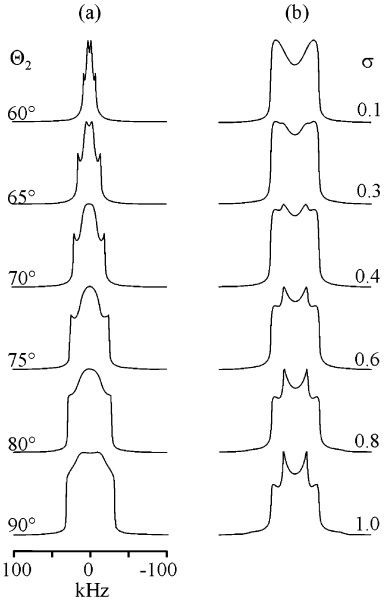

Figure 10. Theoretical ^{2}H NMR spectra (quadrupole echo sequence, $\tau_e = 20$ μs) obtained for two superimposed jump processes. The first rotation (degenerate six-site jumps) is in the fast motional limit, and the angle between the C$-^2$H bond direction and the motional symmetry axis is $\Theta_1 = 90°$. The second motion is a degenerate three-site jump process about a motional symmetry axis. (a) Influence of the opening angle Θ_2 between the first and second motional symmetry axes. The correlation time of the second rotation is 2×10^{-6} s. (b) Influence of a Gaussian distribution of correlation times with varying distribution width σ. The opening angle Θ_2 between the first and second motional symmetry axes is 90°, and the correlation time of the second rotation (center of distribution) is 1×10^{-6} s.

for benzene-d_6/CPZ, the angle Θ_2 is not exactly 90° over the whole temperature range. Rather, it varies slightly with temperature with values between 80° and 90°.

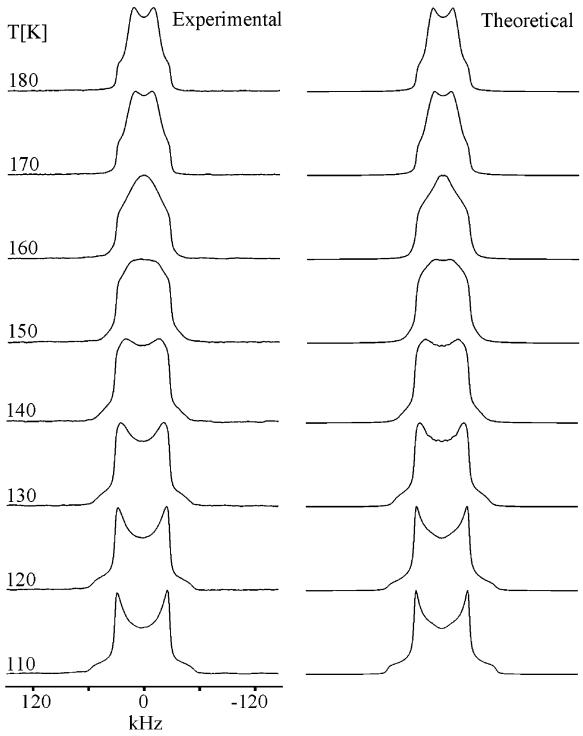

Figure 11. Experimental (left column) and theoretical (right column) ^{2}H NMR spectra ($\tau_e = 20$ μs) of benzene-d_6/CPZ. The theoretical ^{2}H NMR line shapes were obtained by using two superimposed overall rotations: one rotation about the channel long axis (nondegenerate three-site jump process) and the second rotation about the C_6 symmetry axis (degenerate six-site jump process). The simulation parameters are summarized in Figures 12 and 13 and Table 1. The Euler angle Θ_2 was taken to be 90° (110 and 120 K), 87° (130 K), or 85° (140, 150, 160, 170, and 180 K).

TABLE 1: Simulation Parameters Used during ^{2}H NMR Data Analysis

parameter	value
quadrupolar coupling constant[a] (e^2qQ/h)	169 kHz[b] 169−189 kHz[c]
transformation angles (six-site)[d]	
ϕ_1	0°
Θ_1	90°
ψ_1	−120°, −60°, 0°, +60°, +120°, +180°
transformation angles (three-site)[e]	
ϕ_2	0°
Θ_2	80−90°
ψ_2	−120°, 0°, +120°
residual line width ($1/\pi T_2$)	2000 Hz
width of Gaussian distribution σ[f]	0.22

[a] Asymmetry parameter $\eta = 0.05$. [b] Used for spectra simulations at $T \geq 110$ K. [c] Used for spectra simulations at $T < 110$ K. [d] Euler angles ϕ_1, Θ_1, and ψ_1 relating the magnetic principal axis system and molecular axis system 1 (*z* axis parallel to molecular C_6 axis). [e] Euler angles ϕ_2, Θ_2, and ψ_2 relating molecular axis system 1 and the molecular axis system 2 (*z* axis parallel to CPZ channel axis). [f] See eq 7, rotation about channel axis Z_{CH}, 110 K $\leq T \leq$ 180 K).

The aforementioned model assumptions with two superimposed rotations about the molecular C_6 axis (degenerate 60° jumps) and the CPZ channel axis (nondegenerate 120° jumps) were sufficient to provide a quantitative reproduction of the experimental ^{2}H NMR spectra (fixed pulse separation $\tau_e = 20$ μs) in the intermediate temperature range (see Figure 11). The temperature-dependent variables were the motional correlation time τ_{CH}, the opening angle Θ_2, and the population p_1. In addition, a fast overall fluctuation of the benzene guests is

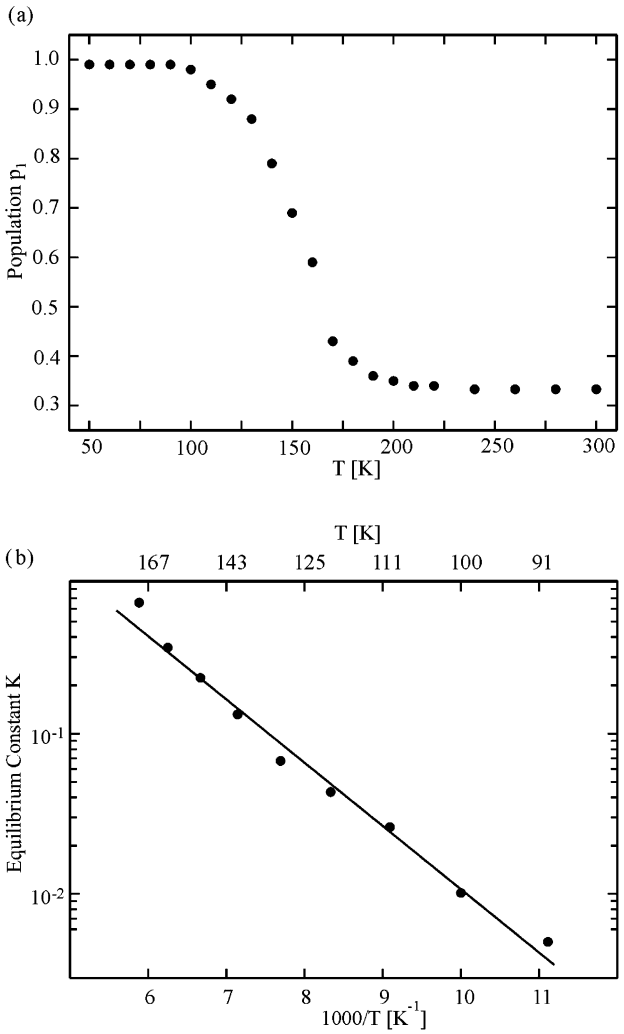

Figure 12. (a) Derived equilibrium population p_1 for the nondegenerate three-site jump process about CPZ channel long axis. (b) Semilogarithmic plot of $K = (1 - p_1)/2p_1$ against inverse temperature.

present that is reflected by the reduced static quadrupolar coupling constant of 169 kHz, used at these elevated temperatures. The corresponding theoretical ^{2}H NMR spectra are shown in Figure 11 (right column). Plots of the population p_1 and the correlation time τ_{CH} as a function of temperature are given in Figures 12a and 13. It should be noted that, for consistency, the simulations also include a Gaussian distribution of correlation times ($\sigma = 0.22$). This is a consequence of the analysis of the partially relaxed spectra (at variable pulse separation τ_e), as discussed in the next paragraph.

The quality of the motional model in the intermediate temperature range was further examined by partially relaxed ^{2}H NMR line shapes from the quadrupole echo experiment at different pulse spacings τ_e (see Figure 6). Extensive model simulations, assuming a single correlation time τ_{CH}, demonstrated that the theoretical signals always decay faster with increasing τ_e than their experimental counterparts. We therefore have tested various other models for the description of the overall reorientation about the CPZ channel long axis (see Experimental Section), but none of them provided better results for the partially relaxed ^{2}H NMR spectra. An improved reproduction of the partially relaxed ^{2}H NMR spectra could be achieved by considering a Gaussian distribution of correlation times (see Experimental Section). Here, model simulations have shown that the actual width of the distribution is crucial for the

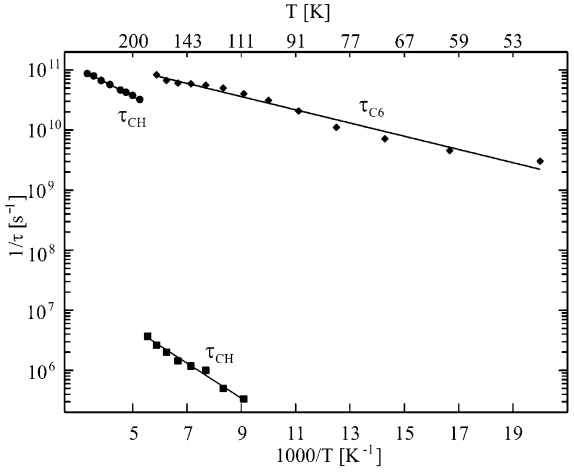

Figure 13. Arrhenius plot for the overall guest motions of benzene-d_6/CPZ: (a) Correlation times for the rotation about the channel axis Z_{CH} (■,●). The squares represent data from analysis of partially relaxed spectra from quadrupole echo experiments, line shape studies, and spin−lattice relaxation data in the intermediate temperature region. The circles represent data from the analysis of the spin−lattice relaxation data in the high temperature region (temperatures above 190 K). (b) Correlation times for the rotation about the C_6 symmetry axis Z_{C6} (◆), as derived from the spin−lattice relaxation data in the intermediate and low temperature regions, i.e., below 190 K.

appearance of the ^{2}H NMR spectra. This is demonstrated in Figure 10 (right column), where theoretical ^{2}H NMR spectra are depicted for a fixed center of the distribution ($\tau_{c,0} = 2 \times 10^{-6}$ s) and various distribution widths. From such model simulations, an upper distribution width of $\sigma = 0.22$ was determined, which then was used for the theoretical reproduction of the ^{2}H NMR line shapes in Figure 11 (fixed $\tau_e = 20$ μs) and the corresponding partially relaxed ^{2}H NMR spectra (see Figure 6). In general, it can be seen that, on the basis of our model assumptions, the overall line shape can be completely reproduced. However, there are still deviations for the relative intensities in the partially relaxed spectra, which we cannot yet explain. The assumption of a distribution of correlation times due to some sample heterogeneity appears to be justified, as the spectral effects at low temperatures between 20 and 40 K were attributed to some distribution of correlation times (here, rotation about the C_6 symmetry axis).

Figure 12a depicts the derived population p_1, characterizing the rotational jumps about the channel axis as a function of temperature. These populations can be further used to calculate the equilibrium constant according to

$$K = \frac{1 - p_1}{2p_1} \tag{9}$$

The semilogarithmic plot of K against the inverse temperature (see Figure 12b) then provides the enthalpy difference ΔH between the jump sites (see Figure 7b). For the present benzene-d_6/CPZ sample, ΔH is found to 7.6 kJ/mol. The derived correlation times τ_{CH} for the rotation of the benzene guests about the CPZ channel long axis are plotted in Figure 13. They follow an Arrhenius behavior from which an activation energy of 5.4 kJ/mol was derived (see Table 2).

The experimental T_{1Z} curve is given in Figure 5. In the present study, we omitted the temperature range below 40 K, which is characterized by the superposition of two spectral components, and solely focused on the temperature range above the T_{1Z} minimum. It is quite obvious that, between 40 and 180 K, T_{1Z}

TABLE 2: Kinetic Parameters Derived from Arrhenius Representation for Benzene-d_6/CPZ Inclusion Compounds

molecular motion	preexponential factor (s^{-1})	activation energy (kJ/mol)
rotation about the channel axis ($T \geq 190$ K)	4.9×10^{11}	4.2 ± 0.1
rotation about the channel axis (110 K $\leq T \leq$ 180 K)	1.3×10^{8}	5.4 ± 0.3
rotation about the molecular C_6 axis ($T \geq 190$ K)	3.5×10^{11}	2.1 ± 0.1

is dominated by the rotation about the molecular C_6 axis, given that the second motional contribution—the rotation about the CPZ channel axis—normally is too slow and does not make a major contribution to spin−lattice relaxation. This conclusion is further supported by the corresponding partially relaxed ^{2}H NMR line shapes from the inversion recovery experiments (see Figure 14, left and center columns), which can be fully described on the basis of this model assumption.

It is worthwhile to note that the simulation of the partially relaxed spectra (inversion recovery spectra) in the intermediate temperature range (see center column in Figure 14, $T = 160$ K), where the rotation about the CPZ channels gives rise to characteristic line shape effects, both spin−lattice and spin−spin relaxations effects had to be included (see Experimental Section). The T_{1Z} data analysis in this temperature range is completely consistent with the aforementioned line shape and T_2 analyses, given that the derived data (i.e., motional correlation times for rotation about channel long axis) from that part are fully taken into account.

The observed inclination of the T_{1Z} curve around 160 K (i.e., decrease of the slope with increasing temperature) can be attributed to the contribution from the rotation of the benzene guests about the CPZ channel axis to spin−lattice relaxation, which becomes increasingly important at higher temperatures. The correlation times for C_6 rotation, derived from the T_{1Z} data analysis up to 180 K, are summarized in Figure 13. The corresponding activation energy is 2.1 kJ/mol.

The spin−lattice relaxation behavior again changes upon entering the high temperature region, which is reflected by a bend in the T_{1Z} curve around 190 K. Extensive model simulations demonstrated that this bend is a result of a dramatic change in the guest mobility, although, as mentioned earlier, there is no evidence from DSC as well as ^{13}C and ^{31}P NMR studies for any substantial structural changes of the CPZ host matrix. It is thus assumed that the T_{1Z} data and the corresponding partially relaxed line shapes (inversion recovery experiment, Figure 14, right column) in the high temperature region above 190 K are now dominated by the rotational motion about the CPZ channel axis (model I), which, however, is about 3 orders of magnitude faster than below 190 K. At the same time, the C_6 rotation also must experience a sudden acceleration in this temperature range. That is, above 190 K, this motion does not contribute any further to spin−lattice relaxation. The derived correlation times for rotation about the channel long axis above 190 K are now on the order of 10^{-11} s, from which an activation energy of 4.5 kJ/mol is derived.

It should be emphasized that a simple extension of the Arrhenius plot for the rotation about the channel long axis from the analysis below 190 K to the region above 190 K (model II) is not consistent with the experimental results, as the rotation about the channel axis—which, below 190 K, is on the order of 10^{-7} s—lies on the low-temperature side of the T_{1Z} curve and approaches the T_{1Z} minimum as the temperature increases. Thus, the temperature dependence of the T_{1Z} data would be opposite

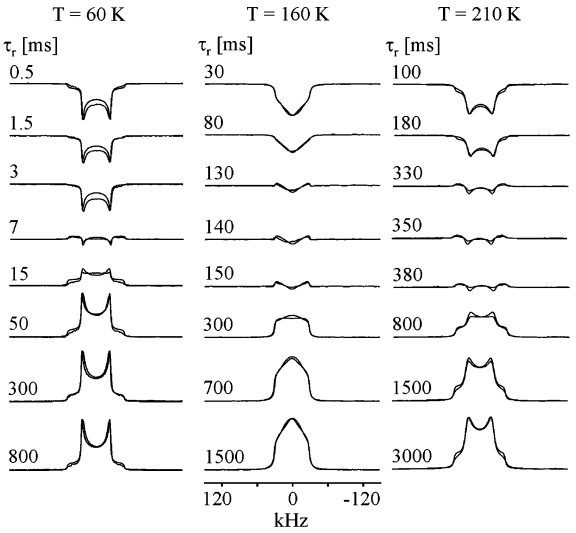

Figure 14. Experimental and simulated partially relaxed spectra obtained from the inversion recovery experiment. The spectra correspond to the high (210 K), intermediate (160 K), and low (60 K) temperature regions. The theoretical spectra at 160 K take into account line shapes effects (characteristic line broadening, nondegenerate six-site jump process) as well as motions in the fast limit (spin−lattice relaxation effects, degenerate six-site jump process). The simulation parameters are summarized in Figures 12 and 13 and in Table 1. The Euler angle Θ_2 was taken to be 90° (60 K), 85° (160 K), or 84° (210 K).

to the experimental observation, and in addition, the theoretical T_{1Z} anisotropy (partially relaxed spectra from inversion recovery experiment) does not match with the experimental findings. If, on the other hand, we simply extend the Arrhenius line of the C_6 rotation from the region below 190 K to temperatures above 190 K (model III), then a consistent data analysis would also be possible, comprising both the reproduction of the T_{1Z} values and the T_{1Z} anisotropy. However, this motional model would yield correlation times for the rotation about the CPZ channel axis between 3×10^{-12} and 3×10^{-14} s (activation energy $\approx$ 24 kJ/mol), i.e., the rotation about the channel axis would be even faster than the C_6 rotation. That is, the overall change of the rate constants at 190 K would be even 5 orders of magnitude, as compared to 3 orders of magnitude for our earlier model I, and a higher activation energy would result as compared to that for the temperature range below 190 K.

On the basis of the present experimental spin−lattice relaxation data for the high temperature region, it is not possible to distinguish between models I and III. However, model I appears to be more reasonable, as the changes of the correlation times at 190 K are less dramatic, and the activation energy is in better agreement with the data derived for the intermediate and low temperature regions (see above).

Two earlier publications dealt with the behavior of the guest molecules in benzene/CPZ inclusion compounds. In the very first work, Allcock and co-workers[37] analyzed broad-line ^{1}H NMR measurements and concluded that the benzene molecules undergo some tumbling motions that can be followed down to 218 K. In a more recent study, Meirovitch and co-workers[38] performed a ^{2}H NMR study on benzene-d_6/CPZ, which, however, only considered NMR line shape effects between 120 and 180 K. The ^{2}H NMR line shape analysis was made with a very similar approach, as discussed in the present work. The authors assumed that the benzene guests undergo a rotation about the C_6 symmetry axis that is fast on the NMR time scale. The observed line shape effects were described by a rotation of the benzene molecules about the CPZ channel symmetry axis

for which a degenerate three-site jump model was used. On the basis of this approach, the authors were able to reproduce their experimental ^{2}NMR line shapes for a fixed pulse delay τ_e = 100 μs, which yielded correlation times in a similar range as those obtained in the present work. The derived activation energy of about 17 kJ/mol, however, was significantly higher than found here. There are several factors that might explain these discrepancies. Hence, the previous study was based solely on the consideration of line shape effects for a fixed τ_e value of 100 μs, which, in addition, was not explicitly taken into account during the data analysis. That is, the line shape simulations were done with the assumption of $\tau_e = 0$ μs, which—as shown above by the examples in Figure 9—can provide severe alterations of the partially relaxed ^{2}H NMR line shapes, depending on the actual motional correlation time. Moreover, the experimental $\pi/2$ pulse lengths of 8 μs in the earlier work causes some ^{2}H NMR line shape distortions[61] that were not explicitly considered.

The derived activation energy for the C_6 rotation of the benzene guests in CPZ can be further compared with the corresponding value reported for solid bulk benzene.[26] The activation energy of 16.5 kJ/mol in bulk benzene is almost 8 times higher than that found for the present CPZ inclusion compound. In addition, for bulk benzene, the C_6 rotation is only detectable above 100 K via line shape effects and relaxation experiments. The overall time scale of this process is thus considerably slower than for the CPZ inclusion compound (shifted by 6 orders of magnitude), which is attributed to the much greater steric hindrance in bulk benzene.

The present results for benzene-d_6/CPZ are consistent with data reported for related guest molecules in CPZ inclusion compounds. For instance, ^{2}H NMR line shape and relaxation studies were reported for 1,3,5-trioxane-d_6 and cyclohexane-d_{12} in cyclophosphazene.[25,28] Here again, various motional contributions can be assigned, namely, (i) rotation about the molecular C_3 axis (rotational diffusion or degenerate three-site jumps), (ii) rotation about the channel axis (degenerate three-site jumps), (iii) overall fluctuations, and (iv) intermolecular ring inversion. The overall rotational motions can again be followed by dynamic NMR methods to temperatures far below 100 K and, in general, are characterized by relatively low activation energies (see Table 3). Nevertheless, the activation energies for both the rotation about the CPZ channel axis and the rotation about the molecular C_3 symmetry axis are higher than for the benzene guests, which can be attributed to the greater steric hindrance of the bulkier aliphatic guest molecules.

For both aliphatic guest species in CPZ, the rotation about the channel long axis can be successfully described by a degenerate three-site jump model. This observation is a consequence of the weaker intermolecular interaction between the aliphatic guest molecules and the CPZ host matrix. In other words, stronger van der Waals interactions are expected between the benzene guests and CPZ host molecules, which might result in a slight distortion of the hexagonal CPZ channel symmetry, as expressed by the nondegenerate three-site jump process (see above). As for the present benzene-d_6/CPZ sample, for steric reasons, the molecular C_3 symmetry axis of the 1,3,5,-trioxane and cyclohexane guests were again found to be oriented perpendicular to the CPZ channel long axis.

Differences between the aliphatic and aromatic guests are found for the ordering behavior. As outlined in refs 22 and 28, the guest ordering, which is affected by only the overall molecular fluctuations, can be described by an order parameter, S_{mol}, that is accessible from the experimental quadrupolar splitting. If such high-frequency fluctuations are present, then the static quadrupolar coupling constant $\nu_{Q,stat}$ has to be replaced by

$$\langle \nu_Q \rangle = \nu_{Q,stat} S_{mol} \tag{10}$$

For the present benzene-d_6/CPZ inclusion compound, S_{mol} lies between 0.89 and 1.0 (data not shown), whereas for 1,3,5-trioxane, values from 0.6 to 1.0 were reported.[28] The considerably higher overall ordering of the benzene guests primarily can be attributed to the stronger nonbonded interactions between the benzene guests and the phenylene rings of CPZ molecules ($\pi-\pi$ interactions), which are not available for the aliphatic guests.

Another ^{2}H NMR study was reported for deuterated 1,3-dioxane in cyclophosphazene,[25] where again rotations about the CPZ channel axis, molecular fluctuations, and internal ring inversions could be assigned. Here, the rotational motion was described by a nondegenerate three-site jump model with an activation energy of 3.9 kJ/mol (see Table 3), which again might indicate some CPZ channel distortion (see above). The motional symmetry axis is located in the symmetry plane of the 1,3-dioxane molecule and is inclined at an angle of 10° with respect to the C$-^2$H bond direction of the equatorial deuterons. Furthermore, it was assumed that the motional symmetry axis is again aligned parallel to the CPZ channel long axis. In this particular case, it was possible to determine the activation energy of the fluctuation process, for which a value of 5.7 kJ/mol was derived.

In addition, the 1,3,5-trioxane, cyclohexane, and 1,3-dioxane guests exhibited intramolecular ring inversions, which are well-known from studies in the liquid and gas phases. Surprisingly, it was found that this intramolecular guest motion is unaffected by the surrounding CPZ matrix. The corresponding activation parameters are thus practically identical to those reported from NMR studies in solution or gas phase.[22,25,28,62]

A further comparison of the derived benzene dynamics can be made with the data from an earlier NMR study on benzene-d_6 included in the 1,3-cyclohexanedione cyclamer.[26] Here, the benzene guests exhibit a behavior quite similar to that reported for bulk benzene. That is, the rotational motion about the C_6

TABLE 3: Activation Energies (kJ/mol) for Various Host−Guest Motions Related to Benzene-d_6/CPZ Inclusion Compounds

compound	rotation about the channel axis	rotation about the molecular axis
bulk benzene[a]		16.5
guest molecules in cyclophosphazene		
benzene-d_6[b]	5.4	2.1
1,3,5-trioxane[c]	10.9	10.0
cyclohexane[d]	8.4	6.1
1,3 dioxane[d]	3.9	
benzene-d_6 in different host systems		
1,3-cyclohexanedione[a]		24.9
KL zeolite[e]		28.0
Na−Y zeolite[f]		23.5
Na−Y zeolite[g]		25.8

[a] Ok, J. H.; Vold, R. R.; Vold, R. L. *J. Phys. Chem.* **1989**, *93*, 7618. [b] This work. [c] Liebelt, A; Detken, A.; Müller, K. *J. Phys. Chem. B* **2002**, *106*, 7781. [d] Liebelt, A.; Tiritiris, I.; Müller, K. *Mol. Cryst. Liq. Cryst.* **2001**, *356*, 527. [e] Sato, T.; Kunimori, K.; Hayashi, S. *Phys. Chem. Chem. Phys.* **1999**, *1*, 3839. [f] Bull, L. M.; Henson, N. J.; Cheetham, A. K.; Newsam, J. M.; Heyes, S. J. *J. Phys. Chem.* **1993**, *97*, 11776. [g] Goncalves, J. A. S.; Portsmouth, R. L.; Alexander, P.; Gladden, L. F. *J. Phys. Chem.* **1995**, *99*, 3317.

symmetry axis is strongly hindered, as reflected by the absolute rate constants and the high activation energy of 24.9 kJ/mol. These findings can be explained by the particular orientation of the benzene guests in the cyclamer cavity, which gives rise to the formation of hydrogen bonds between the benzene molecules and the carbonyl groups of the host lattice.

Finally, the benzene dynamics was also studied for zeolites of comparable channel diameter. For example, the KL zeolite[24] exhibits a channel opening of 7.1 Å diameter. Here, the benzene guests undergo very rapid rotation about their molecular C_6 symmetry axes, which are directed toward the center of the zeolite channel. In addition, the molecules execute a six-site jump process about the channel among equally populated jump sites that are defined by the position of the K^+ ions. The activation energy for this latter motion is reported to be 28.0 kJ/mol. Similar values have been reported for the benzene reorientation in another zeolite, NaY (23.5 kJ/mol,[63] 25.8 kJ/mol[64]), which exhibits a structure similar to that of the KL zeolite. The large activation energy for the benzene reorientation in KL zeolite was attributed to the interaction between the K^+ ions and the π electrons in benzene.

Conclusions

The molecular dynamics and ordering characteristics of perdeuterated benzene, trapped in the hexagonal channels made from tris(1,2-dioxyphenyl)cyclotriphosphazene, were studied by dynamic ^{2}H NMR spectroscopy covering a temperature range from 20 K to room temperature. The analysis of the experimental data revealed highly mobile benzene molecules, despite the highly confined conditions. The guest molecules undergo various types of superimposed motions, namely, rotation about the cyclophosphazene channel long axis, fast rotation about the C_6 symmetry axis of the benzene molecules, and overall fluctuations. The rotational motion about the cyclophosphazene channels affects the experimental ^{2}H NMR line shapes and both spin−spin and spin−lattice relaxation in the intermediate and high temperature regions, whereas the much faster rotation about the C_6 symmetry axis dominates spin−lattice relaxation at low and intermediate temperatures. Furthermore, it is found that the two rotational symmetry axes are almost perpendicular to each other. The higher overall guest ordering is related to stronger guest−host interactions of the benzene-d_6/CPZ inclusion compound. The present results are consistent with the data reported earlier for related compounds. An open question is the molecular origin of the dramatic change of the guest mobility around 190 K, which, according to the available experimental data, is not related to a solid−solid phase transition. Here, variable-temperature single-crystal X-ray studies could certainly provide information about the presence of some subtle changes of the CPZ channel structure that are not detectable with our available experimental methods. In general, it could be demonstrated that a comprehensive analysis of such dynamic ^{2}H NMR experiments provides a detailed picture of the features of the guest species in such inclusion compounds and the impact of nonbonded interactions on these molecular parameters.

Acknowledgment. We thank Mrs. D. Zauser and Mrs. G. Bräuning for the synthesis of cyclophosphazene used in the present work. Financial support from the Deutsche Forschungsgemeinschaft and the Graduiertenkolleg "Modern Methods of Magnetic Resonance in Materials Science" is gratefully acknowledged.

References and Notes

(1) Atwood, J. L., Davies, J. E. D., MacNicol, D. D., Eds. *Inclusion Compounds*; Academic Press: New York, 1984; Vols. 1−3. Atwood, J. L., Davies, J. E. D., MacNicol, D. D., Eds. *Inclusion Compounds*; Oxford University Press: Oxford, U.K., 1991; Vols. 4 and 5.

(2) Atwood, J. L., Davies, J. E. D., MacNicol, D. D., Vögtle, E., Eds. *Comprehensive Supramolecular Chemistry*; Pergamon Press: London, 1996.

(3) Schlenk, W. *Liebigs Ann. Chem*. **1949**, *204*, 565; *Liebigs Ann. Chem*. **1951**, *573*, 142.

(4) Krasnov, A. A.; Klimenok, B. V.; Telle, V. I. *Zh. Fiz. Khim*. **1977**, *51*, 294; *Chem. Abstr*. **1977**, *86*, 188931.

(5) Ripmeester, J. In *Inclusion Compounds*; Atwood, J. L., Davies, J. E. D., MacNicol, D. D., Eds.; Oxford University Press: Oxford, U.K., 1991; Vol. 5, p 37.

(6) Hollingsworth, M. D.; Harris, K. D. In *Comprehensive Supramolecular Chemistry*; Atwood, J. L., Davies, J. E. D., MacNicol, D. D., Vögtle, E., Eds.; Pergamon Press: London, 1996; Vol. 6, p 177.

(7) Fukushima, K. *J. Mol. Struct.* **1976**, *34*, 67.

(8) Fukushima, K.; Sugiura, K. *J. Mol. Struct.* **1977**, *41*, 41.

(9) Gilson, D. R. F.; McDowell, C. A. *Mol. Phys*. **1961**, *4*, 125.

(10) Bell, J. D.; Richards, R. E. *Trans. Faraday Soc*. **1969**, *65*, 2529.

(11) Clément, R.; Mazieres, C.; Gourdji, M.; Guibé, L. *J. Chem. Phys*. **1977**, *67*, 5381.

(12) Gustavsen, J. E.; Klaeboe, P.; Kvila, H. *Acta Chem. Scand., Ser. A* **1978**, *32*, 25.

(13) Allen, A.; Fawcett, V.; Long, D. A. *J. Raman Spectrosc.* **1976**, *4*, 285.

(14) Schmider, J.; Müller, K. *J. Phys. Chem. A* **1998**, *102*, 1181.

(15) Griffin, R. G. *Methods Enzymol*. **1981**, *72*, 108.

(16) Davis, J. H. *Biochim. Biophys. Acta* **1983**, *737*, 117.

(17) Spiess, H. W. *Adv. Polym. Sci.* **1985**, *66*, 23.

(18) Müller, K.; Meier, P.; Kothe, G. *Prog. Nucl. Magn. Reson. Spectrosc.* **1985**, *17*, 211.

(19) Vold, R. R.; Vold, R. L. *Adv. Magn. Opt. Res.* **1991**, *16*, 85.

(20) Greenfield, M. S.; Vold, R. L.; Vold, R. R *Mol. Phys.* **1989**, *66*, 269.

(21) Meirovitch, E.; Krant, T.; Vega, S. *J. Phys. Chem.* **1983**, *87*, 1390.

(22) Poupko, R.; Furman, E.; Müller, K.; Luz, Z. *J. Chem. Phys.* **1991**, *95*, 407.

(23) Meirovitch, E.; Belsky, I. *J. Phys. Chem.* **1984**, *88*, 4308.

(24) Sato, T.; Kunimori, K.; Hayashi, S. *Phys. Chem. Chem. Phys*. **1999**, *1*, 3839.

(25) Liebelt, A.; Tiritiris, I.; Müller, K. *Mol. Cryst. Liq. Cryst*. **2001**, *356*, 527.

(26) Ok, J. H.; Vold, R. R.; Vold, R. L. *J. Phys. Chem*. **1989**, *93*, 7618.

(27) Aliev, A. E.; Harris, K. D. M. *J. Phys. Chem*. **1995**, *99*, 1156.

(28) Liebelt, A.; Detken, A.; Müller, K. *J. Phys. Chem. B* **2002**, *106*, 7781.

(29) Wefing, S.; Kaufmann, S.; Spiess, H. W. *J. Chem. Phys*. **1988**, *89*, 1234.

(30) Schmidt, C. Blümich, B.; Spiess, H. W. *J. Magn. Reson.* **1988**, *79*, 269.

(31) Schmidt-Rohr, K.; Spiess, H. W. *Multidimensional Solid-State NMR and Polymers;* Academic Press: London, 1988.

(32) Allcock, H. R. In *Inclusion Compounds*; Atwood, L. J., Davies, J. E. D., MacNicol, D. D., Eds.; Academic Press: New York, 1984; Vol. 1, p 351.

(33) Allcock, H. R. *Acc. Chem. Res.* **1978**, *11*, 81.

(34) Allcock, H. R. *J. Am. Chem. Soc.* **1964**, *86*, 2591.

(35) Allcock, H. R.; Siegel, L. A. *J. Am. Chem. Soc*. **1964**, *86*, 5140.

(36) Allcock, H. R.; Stein, M. T. *J. Am. Chem. Soc*. **1974**, *96*, 49.

(37) Allcock, H. R.; Allen, R. W.; Bissell, E. C.; Smeltz, L. A.; Teeter, M. *J. Am. Chem. Soc.* **1976**, *98*, 5120.

(38) Meirovitch, E.; Belsky, I.; Vega, S. *J. Phys. Chem.* **1984**, *88*, 1522.

(39) Meirovitch, E.; Rananavare, S. B.; Freed, J. H. *J. Phys. Chem.* **1987**, *91*, 5014.

(40) Meirovitch, E. *J. Phys. Chem.* **1984**, *88*, 6411.

(41) Allcock, H. R.; Kugel, R. L. *Inorg. Chem*. **1966**, *5*, 1016.

(42) Smith, B. T.; Boyle, J. M.; Garbow, B. S.; Ikebe, Y.; Klema, V. C.; Moler, C. B. *Matrix Eingensystem Routines−EISPACK Guide*, Springer-Verlag: Berlin, 1976.

(43) Wittebort, R. J.; Olejniczak, E. T.; Griffin, R. G. *J. Chem. Phys*. **1987**, *86*, 5411.

(44) Spiess, H. W.; Sillescu, H. *J. Magn. Reson*. **1982**, *42*, 381.

(45) Wangness, R. K.; Bloch, F. *Phys. Rev*. **1953**, *89*, 728.

(46) Redfield, A. G. *Adv. Magn. Reson.* **1965**, *1*, 1.

(47) Redfield, A. G. *IBM J. Res. Dev*. **1953**, *1*, 19.

(48) Wittebort, R. J.; Szabo, A. *J. Chem. Phys*. **1978**, *69*, 1722.

(49) Torchia, D. A.; Szabo, A. *J. Magn. Reson*. **1982**, *42*, 107.

(50) Beshah, K.; Olejniczak, E. T.; Griffin, R. G. *J. Chem. Phys*. **1987**, *86*, 4730.

(51) Allcock, H. R.; Levin, M. L.; Whittle, R. R. *Inorg. Chem*. **1986**, *25*, 41.

(52) Comotti, A.; Simonutti, R.; Stramare, S.; Sozzani, P. *Nanotechnology* **1999**, *10*, 70.

(53) Kubono, K.; Asaka, N.; Isoda, S.; Kobayashi, T. *Acta Crystallogr. C* **1993**, *49*, 404.

(54) Power, W. P.; Wasylishen, R. E.; Curtis, R. D. *Can. J. Chem*. **1989**, *67*, 454.
(55) Gedat, E.; Schreiber, A.; Albrecht, J.; Emmler, Th.; Shenderovich, I.; Findenegg, G. H.; Limbach, H.-H.; Buntkowsky, G. *J. Phys. Chem. B* **2002**, *106*, 1977.
(56) Schwartz, L. J.; Stillman, A. E.; Freed, J. H. *J. Chem. Phys*. **1982**, *77*, 5410.
(57) Millhauser, G. L.; Freed, J. H. *J. Chem. Phys*. **1984**, *81*, 37.
(58) Vold, R. R. In *NMR Probes of Molecular Dynamics*; Tycko, R., Ed.; Kluwer Academic Publishers: Dordrecht, The Netherlands, 1994; p 27.
(59) Wemmer, D. E. Ph.D. Thesis, University of California, Berkeley, CA, 1978.
(60) Bloom, M.; Davis, J. H.; Valic, M. I. *Can. J. Phys*. **1980**, *58*, 1510.
(61) Rice, D. M.; Wittebort, R. J.; Griffin, R. G.; Meirovitch, E.; Stimson, E. R.; Meinwald, Y. C.; Freed J. H. *J. Am. Chem. Soc*. **1981**, *103*, 7707.
(62) Gelerinter, E.; Luz, Z.; Poupko, R.; Zimmermann, H. *J. Phys. Chem*. **1990**, *94*, 8845.
(63) Bull, L. M.; Henson, N. J.; Cheetham, A. K.; Newsam, J. M.; Heyes, S. J. *J. Phys. Chem.* **1993**, *97*, 11776.
(64) Goncalves, J. A. S.; Portsmouth, R. L.; Alexander, P.; Gladden, L. F. *J. Phys. Chem.* **1995**, *99*, 3317.